Crustal and Uppermost Mantle Velocity Structure of Northern Eurasia along the Profile Quartz

Article *in* Bulletin of the Seismological Society of America · April 1997

CITATIONS
29

READS
70

3 authors, including:

Scott B. Smithson
University of Wyoming
177 PUBLICATIONS **3,973** CITATIONS

SEE PROFILE

Bulletin of the Seismological Society of America, Vol. 87, No. 2, pp. 414–426, April 1997

Crustal and Uppermost Mantle Velocity Structure of Northern Eurasia along the Profile Quartz

by Werner Schueller,* Igor B. Morozov, and Scott B. Smithson

Abstract The velocity structure of the crust and uppermost mantle beneath the DSS profile *Quartz* in northwestern Russia is determined using a linearized seismic tomography scheme. The analysis is performed on the northern 2200 km of the profile spanning from the Kola Peninsula, the Timan–Pechora basin, and the Uralian fold belt to the west Siberian basin. Refracted and reflected phases recorded from 28 chemical and two nuclear shot points are analyzed.

The inversion technique allows determination of the *P*-wave velocity structure and estimation of the depth of the crust–mantle discontinuity. Resolution analysis shows that the upper crustal structure and sections of the lower crust and uppermost mantle are well resolved. The modeled velocity and crustal thickness anomalies are confirmed by the resulting structure of the resolution matrix. Poorer ray coverage in parts of the lower crust and most sections of the uppermost mantle limits their resolvable structures.

A thick (over 10 km), high-velocity block ($V_p > 7.0$ km/sec) in the lower crust of the Precambrian beneath the Kola Peninsula; crustal thinning and a wide range of compressional velocities in the sedimentary basin structures; and a significant crustal root beneath the Uralian fold belt (42 to 45 km Moho depth with high lower crustal velocities exceeding 7.0 km/sec) were identified in the tectonic structure of northwestern Eurasia.

Introduction

The continental seismic profile *Quartz* (also known as *Murmansk-Kizil* profile) was acquired between 1984 and 1987 spanning 3950 km from northeastern Fennoscandia to central Asia (Fig. 1). The profile is a part of the extensive deep seismic sounding (DSS) program of the former USSR covering more than 150,000 km of seismic lines in northern Eurasia (Egorkin *et al.*, 1991; Kozlovsky, 1990; Benz *et al.*, 1992). Large chemical explosions as well as peaceful nuclear explosions (PNEs), used since the 1970s, were set up along profiles with offset ranges often exceeding 3000 km.

Using two-dimensional travel-time refraction/reflection tomography, we derive the *P*-wave velocity structure of the crust and uppermost mantle to a depth of 60 km under the northwestern part of the transect. We use crustal and upper mantle refractions and reflections from the Moho produced by 28 chemical and 2 nuclear shots for iterative construction of a velocity–interface model. The tomographic inversion scheme allows evaluation of obtained model resolution.

Earlier interpretations of the Quartz data include a crustal model designed by the Center for Regional Geophysical and Geoecological Research (GEON), Moscow, Russia, and one-dimensional modeling of the upper mantle structure using forward methods (Egorkin and Mikhaltsev, 1990; Egorkin, 1992; Benz *et al.*, 1992; Mechie *et al.*, 1993). Recently, Ryberg *et al.* (1996) proposed a combined two-dimensional model of the upper mantle based on forward travel-time modeling of all three nuclear shots. Three nuclear shots spaced at a distance of about 1000 km between them, however, do not provide a sufficient ray coverage for a 2D interpretation, and a great ambiguity in the obtained mantle velocity still remains. In the uppermost part of the mantle, however, this ambiguity can be strongly alleviated by the analysis of the chemical explosion data.

Using shot records from chemical explosions, GEON developed a two-dimensional crustal model following the block-layer approach typical for most DSS interpretations of Russian data. This model shows a detailed block structure containing a large number of vertical and horizontal velocity contrasts, as well as small-scale zones of velocity inversion. The model contains a large number of dipping faults separating upper and lower crustal blocks of different physical properties. The Moho is offset by fault systems creating a discontinuous crustal–mantle interface. Some reflecting horizons cut the Moho and extend all the way into the mantle.

*Present address: Grant Geophysical, Park Row, 10, Houston, Texas.

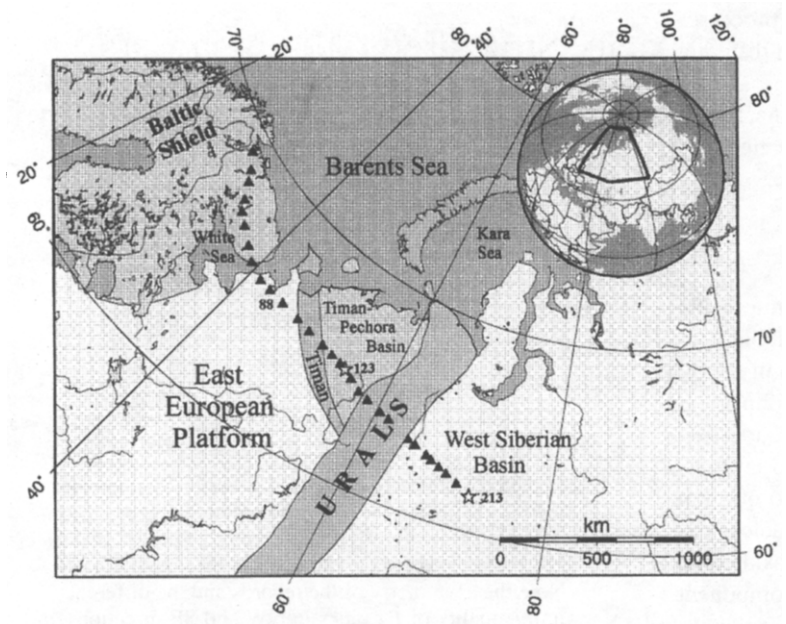

Figure 1. Northern and central sections of the profile Quartz. This 2250-km-long segment includes 28 chemical (triangles) and 2 nuclear shot points (stars). Main tectonic units and the numbers of the shots referred in the text are indicated.

The present study is the first attempt since the original GEON interpretation to analyze the crustal part (48 chemical shots along the entire profile) of the Quartz dataset. Our reinterpretation is mainly motivated by the desire for an independent estimate for the crustal velocity model using advanced inversion techniques. A comprehensive crustal velocity model is necessary to further determine upper mantle velocity structure, and to understand the propagation of regional phases, especially *Lg*, along this transect. Most importantly for the interpretation of this comparatively sparse data set, our inversion scheme allows the evaluation of model quality, including the estimates of spatial resolution and parameter variance.

Geologic and Tectonic Setting

The tectonic units of northern Eurasia crossed by the profile represent a wide variety of continental structures: Archean cratons, ancient platform regions, Hercynian orogens, large extensional basins with thick sedimentary cover, as well as active fold belts with complicated, thick crustal structures. The tectonic units covered by this study are from the northwest to the southeast: the east European platform, including the Baltic shield; the Timan fold belt; the Timan–Pechora basin; the Uralian fold belt; and the west Siberian basin (Fig. 1). The east European platform consolidated at the end of the middle Proterozoic after accretion of smaller continental blocks that joined along suture zones forming a stable craton structure (Zonenshain *et al.,* 1990). The last significant event affecting the platform resulted in granitic intrusions at 1.5 Ga, leaving the craton virtually intact since. The Precambrian Baltic shield is the most stable and the oldest part of the east European platform, with increasing structural ages from the southwest to the northeast. Subduction processes and arc–continent and continent–continent collisions closed an early Proterozoic sea forming the narrow, discontinuous, upthrust Imandra–Varzuga belt along the central Kola Peninsula (Berthelsen and Marker, 1986). The late Precambrian Timan fold belt is an uplift of the Riphean basement of the Timan–Pechora platform. The large sedimentary basin structures of northern Eurasia were formed by deep erosion of the underlying Precambrian and Paleozoic basement followed by subsidence due to the extension of the continental crust within aulacogens or rifts (Zonenshain *et al.,* 1990). The Quartz profile crosses the southern Timan–Pechora basin containing early Devonian to late Cretaceous and early Paleogene sedimentary rocks that range from 3 to 7 km in thickness. The Urals represent a linear collisional fold belt formed at the end of the Paleozoic and at the beginning of the Mesozoic. It developed out of a sequence of oceanic closing, subduction of oceanic crust under island arcs, convergence of lithospheric plates, and continental collision (Zonenshain *et al.,* 1990). Bordering the northeast of the Uralian fold system, the west Siberian basin is one of the world's largest known platform structures. The basement was formed by Paleozoic fold structures of various ages and older Precambrian blocks (Zonenshain *et al.,* 1990). Thick Cenozoic and Mesozoic sedimentary rocks cover the underlying basement.

According to existing models, the continental crust of the former USSR is described as composed of an extremely nonuniform, heterogeneous, block-layered structure bounded by large-scale faults and fracture zones (Volkov *et al.,* 1984; Pavlenkova, 1992). The fault zones are considered to have been the sites of repeated and intensive tectonic-magmatic activity. The origin of the block structure is explained by the deformation of the early plastic lithosphere and subsequent fracturing and by fault development in the

consolidated crust (Nalivkina *et al.,* 1987). These processes created a complex system of lithospheric blocks of different size and orientation. The block-layered model approach resulted mostly from the interpretation of the DSS data, which provided an understanding of characteristic features of northern Eurasia.

Data

We applied the tomographic inversion scheme to the northern 2250 km of the profile, using the available data digitized by that time. Figure 1 shows the location of the 30 shot points input in our analysis (28 chemical and 2 nuclear shots). The average spacing of the shot points is approximately 100 km. Receiver stations were positioned at intervals of 10 to 15 km. Recording ranges span up to 600 km for chemical explosions and over 3000 km for nuclear explosions, providing velocity information to considerable depths of the upper mantle (Figs. 2 and 3). Three-component analog seismic-recording systems were used during the experiment. Digitization of the full record length (nearly 600 sec for nuclear explosions) was performed by GEON at sample intervals of 20 msec.

Crustal refracted waves (*Pg*) as well as the waves turning in the upper mantle (*Pn*) can be seen in most records at offsets exceeding 150 to 250 km. Not all shot records allow clear identification of reflections from the Moho discontinuity (*PmP*). *PmP* is commonly characterized by strong amplitudes at critical distances (90 to 130 km) and is virtually absent at near offsets (Figs. 2 and 3; see also Egorkin and Pavlenkova, 1981).

Figures 2 and 3 show two examples of the shot records. Shot 88 (Fig. 2) is located in the northeastern section of the east European platform between the Kola Peninsula and the Timan belt. Offsets range up to 300 km on both sides of the spread, which extends from the White Sea to the southern Timan–Pechora basin. *Pg* phases are present up to 150 km. While *Pn* continues with strong arriving amplitudes, *PmP* is not easy to identify. Shot 123 (Fig. 3) is the northern nuclear explosion and is located approximately in the middle of the profile used in this study. This shot is located in the southern Timan–Pechora basin. *Pg* extends to about 160 km followed by *Pn* thereafter. Clear *PmP* arrivals span from 40 to 300 km in the west, while Moho reflections in the east interfere with a strong lower crustal reflection and are harder to identify at smaller offsets.

Travel-time picking of refracted and reflected phases was performed from frequency-filtered raw shot gathers. Although differing in some detail, our resulting travel-time curves for *PmP* show a good correspondence to those determined by the center GEON. The differences can be attributed to the use of nonlinear velocity filtering routinely used in GEON data processing. We did not employ this procedure in our analysis, because we found this technique not reliable due to the strong spatial aliasing of the records.

We estimated picking errors by considering the dominant period of the signal and the overall data uncertainty. The presence of various sources of error (including, in some cases, timing and position uncertainties and spatial aliasing) not directly related to the picking procedure caused travel-time errors to commonly exceed the theoretical limit of one-quarter of the dominant period (100 to 150 msec for the considered signal bandwidth). Estimated travel-time errors range from ± 100 to ± 150 msec for near-offset *Pg* and ± 150 to ± 400 msec for *Pn*. The estimated uncertainty for

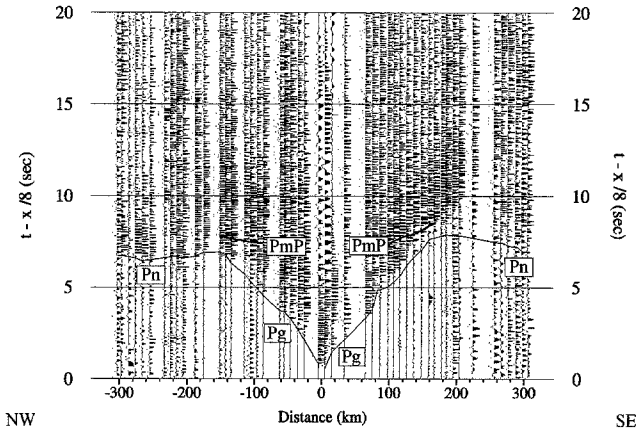

Figure 2. Trace-normalized vertical-component record section for chemical shot point 88, plotted with reduction velocity of 8 km/sec, high pass filter of 1.5 Hz. Picked phases are indicated as *Pg*, *Pn*, and *PmP*. Note the asymmetry of the records and the difference in the quality of *Pn* picks in NW and SE directions.

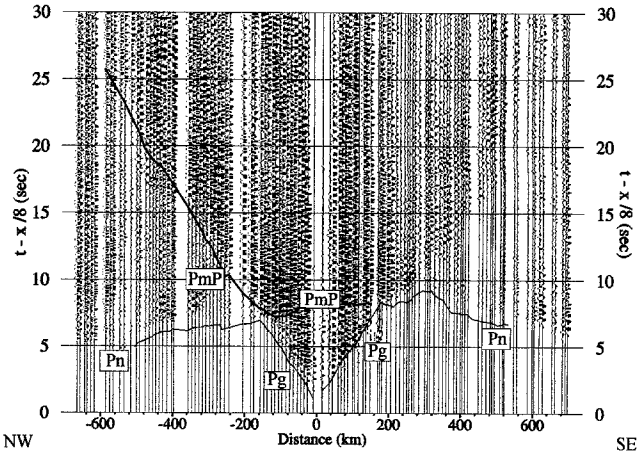

Figure 3. Trace-normalized record section of vertical-component data for nuclear shot point 123, plotted with reduction velocity of 8 km/sec, high pass filter of 1.5 Hz. In our analysis, we used only a part of full offset range (over 2800 km). Picked phases are indicated as *Pg*, *Pn*, and *PmP*. Due to high energy of the shot, seismic phases are observed at far offsets. At the same time, picking of *PmP* is complicated by the interferences with lower crustal reflections, as in the SE part of this shot gather.

PmP was set equal to ±500 msec, corresponding to the larger uncertainty in picking this phase. Some substantial ambiguity in picking *PmP* reflections from the nuclear shot point 213 still remains, since virtually no *PmP* events could be found in the nearby chemical shot records, and reciprocity could not be established.

Travel-Time Inversion for Velocity–Interface Structure

We applied a linearized tomographic refraction/reflection travel-time inversion method based on the algorithm by D. White (1989). This method is designed to invert surface-to-surface refraction and wide-angle reflection data. The inversion scheme allows the determination of velocity inhomogeneities as well as subsurface interface geometries. Each step of the iteration includes two-point raytracing using a shooting method and solving the resulting linear system that relates travel-time variations to the velocity and interface depth perturbations. Details of the algorithm can be found in White (1989). White and Clowes (1990) and White and Boland (1991) describe applications of the technique to marine and continental data sets, respectively.

The velocity field is defined on a uniform, rectangular grid of velocity values. Each of these rectangular cells is divided into two triangular cells, creating a continuous velocity field across the neighboring grid cells. Interface depths are defined at intervals equal to the horizontal node spacing. Refracted rays penetrate the crust predominantly horizontally; therefore, we expect better vertical than horizontal resolution. This results in choosing a larger horizontal (50 km) than vertical (3 km) grid spacing. The choice of the grid is influenced by the density of the shots and receivers and by the expected spatial resolution of the seismic data. We preferred to avoid an excessive overparameterization of the model, because it can lead to a strong dependence of the results on the employed regularization scheme.

Chosen velocity model paramet-rization resulted in a slightly underdetermined linear system. The use of damping during the inversion limited the shape and size of model perturbations that are ill constrained by the travel-time data.

For the inversion of the resulting linear system, we use the LSQR algorithm (Paige and Saunders, 1982), which is particularly designed for solving large, sparse, and asymmetric linear systems. It was developed to seek the least-squares solution of a set of linear equations. Numerical experiments and applications to real data sets have shown that this algorithm is superior in solving ill-conditioned, underdetermined systems compared to other row-action methods such as SIRT and ART (van der Sluis and van der Vorst, 1987; Scales, 1987; Spakman and Nolet, 1988; Nolet, 1993, 1985). However, the LSQR algorithm does not provide a resolution and variance estimate for the resulting solution. Several alternatives to obtain model resolution and covariance estimates are the singular-value decomposition (SVD), impulse responses for localized model resolution (White and Clowes, 1990), resampling technique resulting in model variance estimates (Tichelaar and Ruff, 1989), or construction of an analog of SVD resolution matrix from the orthonormal basis produced by LSQR (Zhang and McMechan, 1995). We used the SVD method in our analysis.

Carefully choosing a realistic starting model close to the actual lithospheric structure reduces the necessary number of iterations and helps to avoid instabilities during the inversion. We used a simplified version of the model by Egorkin and Mikhaltsev (1990). Construction of the starting model involved use of mean upper and lower crustal and uppermost mantle velocities to find appropriate velocity gradients. The Moho boundary was smoothed to a continuous, faultless interface.

Velocity–Interface Inversion Procedure

The linear system is solved for velocity perturbations or interface depth perturbations. Regularization is performed in a typical manner for LSQR, using a single damping parameter (White, 1989). Before updating the model, several solution and model-processing operations are available. Velocity updates are clipped within the range ±0.1 km/sec and smoothed using a three-point moving average operator. While constraining the magnitudes of model perturbations has an effect similar to the damping of the linear system (Zhou *et al.,* 1993), it provides an advantage of a selective and interactive control of the strongest velocity–interface depth instabilities. The resulting model update is input into a new iteration step starting over with raytracing through the new model. The iteration process is terminated as soon as no further improvement in data misfit is obtained or the resulting rms travel-time misfit is less than the estimated travel-time uncertainty, while the magnitude of the χ^2 criterion is approaching the number of travel-time picks.

Exploiting the much higher ray coverage in the upper crust, the first two iterations determined the uppermost crustal structure represented by the first four rows of the starting model corresponding to the upper 9 km of the crust. Only rays turning in the uppermost crust were used at this stage. During the subsequent iterations, we kept the uppermost crustal velocity structure constant, and we inverted for the deeper lithospheric structure and depth of the Moho discontinuity, using far-offset refractions and reflections from the Moho.

The iterations resulted in a final model (Fig. 4) with rms misfit of 221 msec and χ^2 of 1340. Unfortunately, the shooting algorithm was not able to find the geometry of some ray paths in the areas with substantial lateral velocity gradients. This undesirable behavior could be suppressed by additional smoothing of the model and by increased damping during the inversion. The latter operations, however, degrade the resolution of the velocity model and were used very moderately. The percentage of travel-time picks within the chosen offset range that were actually included in the inversion varied from 83% to 97% during different iterations. Additional iterations of interface perturbations did not reduce the

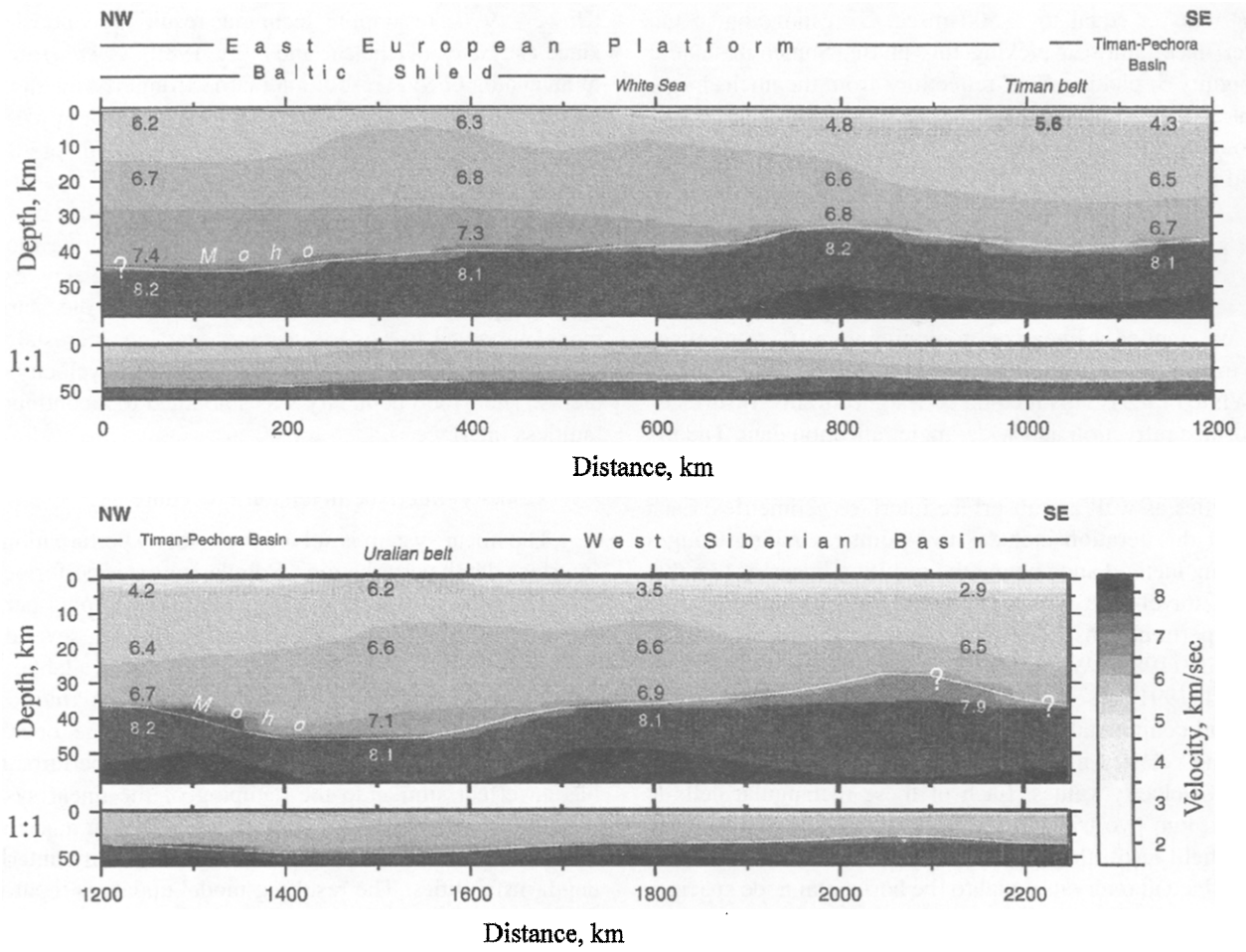

Figure 4. Modeled *P*-wave velocity structure for the crust and uppermost mantle, shown in two parts split at 1200 km. Major tectonic units crossed by the profile are indicated along the distance axis. Characteristic values of *P*-wave velocities are given in labels. Bottom: The velocity model with no vertical exaggeration. Moho depth at the edges of the model is not constrained by the present modeling.

data misfit substantially without introducing a very rough Moho topography, which also limited the number of traceable rays significantly. The averaged misfit is close to the estimated picking error of most of the observed travel times. Although estimated travel-time uncertainties for near offset refractions (*Pg*) are in general smaller than the resulted rms misfit, *PmP* reflections and upper mantle refractions (*Pn*) show a higher average uncertainty, in many cases exceeding the corresponding picking error.

The rms misfit of our final model is larger than that obtained in other studies using similar approaches (e.g., Lutter and Nowack, 1990; Braile *et al.,* 1994). This difference can be attributed to considerably larger model dimensions, nonuniform ray coverage, and relatively wide shot and receiver spacings in the Quartz data.

The modeled *P*-wave velocity structure in the upper lithosphere and the crustal thickness are shown in Figure 4. The continental crust in northwestern Eurasia determined by our tomographic inversion shows major lateral inhomogeneities and significant variations in the depth of the Moho discontinuity. The Kola province in the northeastern Baltic shield is characterized by a high uppermost crustal velocity of 6.2 to 6.3 km/sec. The upper crust below the northernmost part of the profile shows slightly lower velocities than in the southern part of the peninsula. The lower crust is characterized by a thick block of high velocity exceeding 7.0 km/sec at about 28 km depth. Maximum *P*-wave velocities reach 7.4 km/sec in the far northern part of the profile, while they decrease to 7.2 km/sec in the southeastern Kola Peninsula. The depth of the Moho varies from 40 to 45 km, being shallower in the southeast. The thickness of the high-velocity zone in the crust ($V_p > 7.0$ km/sec) reaches about 18 km in the northwest and 11 km in the southeast. Modeled upper mantle velocities range from 8.1 to 8.2 km/sec. For constant crustal depths, *P*-wave velocities decrease from the northeastern Baltic shield toward the Timan belt. Lower-crustal velocities range from 6.6 to 6.8 km/sec. The Moho shallows to 33 km at profile distance of 800 km with upper mantle

velocities of 8.1 to 8.2 km/sec. Further south, the crustal thickness increases to reach a local maximum beneath the Timan belt of 39 km. An area of low velocity compared to the Baltic shield and the west Siberian basin characterizes the crust of the Timan belt and the Timan–Pechora basin. Velocities in the upper consolidated crust range from 5.9 to 6.2 km/sec and reach relatively low values of 6.6 to 6.7 km/sec in the lowermost crust. A slight depression of the Moho interface below the Timan belt is followed by crustal thinning beneath the basin to 35 to 37 km. The Uralian fold belt region shows a relatively high crustal velocity and a thick crust. One of the pronounced features in the resulting model is the crustal root beneath the Uralian fold belt. Although the bottom of the Uralian root is not sampled by the reflected waves, both of its slopes are well constrained by *PmP* and *Pn* phases. The depth of the Moho in this region is 46 km, corresponding to lower crustal velocity of 7.1 km/sec, and the upper mantle velocity is 8.1 km/sec. Modeled velocity values for the upper crust range from 6.2 km/sec a few kilometers below the surface to 6.3 and 6.6 km/sec deeper in the upper crust.

The southeastern part of the profile models the west Siberian basin with a relative thick sedimentary layer of 4 to 5 km and velocities of 2 to 3 km/sec. Consolidated crustal basement velocities range from 6.3 km/sec in the upper crust to 6.8 km/sec in the lower crust. Upper mantle velocities range from 7.9 to 8.0 km/sec with a crustal thickness of about 35 km southeast of the Urals. A prominent uplift of the Moho interface, reaching a minimum of 28 km depth at profile distance of 2100 km, is not supported by current geologic models and is not present in earlier interpretations of the Quartz data. It is only constrained by *PmP* picks of the three most southern shot points. Although modeled as the Moho interface in this study, it may in fact represent a reflection from a lower crustal boundary.

The ray density in the final model is shown in Figure 5. As expected, the ray coverage is nonuniform laterally and vertically; in particular, a much higher ray density resulted for the upper crust compared to the lower crust and the uppermost mantle. Significant gaps in the coverage exist below the White Sea area and beneath the Urals, as well as along the edges of the model. The most dense ray coverage is found in the upper crust at the central Kola Peninsula, the Timan–Pechora basin, and the west Siberian basin with maximum cell counts of 20 to 43. The coverage of the uppermost mantle is limited by the relatively small number of *Pn* events. Figure 6 shows refracted (*Pg*, *Pn*) and reflected (*PmP*) rays and travel times obtained by raytracing in the final velocity–interface model.

Resolution Analysis

The resolving power of a tomographic analysis is defined as its capability to recover the true velocity field and interface geometry. The ray coverage of our final velocity–interface model (Fig. 5) shows that the edges of the model are unconstrained and the resolution of the crust is better than that of the uppermost mantle. Independent sampling of grid cells by rays at different angles contributes to the resolution of the imaged velocity structure. Limited angular coverage results in resolution smearing along the dominant direction of ray penetration. Additional gaps in the ray field, especially below the White Sea area (Fig. 5), cause localized gaps in model resolution.

LSQR matrix inversion does not provide resolution estimates. The model resolution, however, is a function of the model itself and of the corresponding ray coverage (more specifically, it is a function of the Jacobian matrix of the model) but not of the way the model has been obtained. Thus, different techniques can be employed to estimate the sensitivity of the solution to the perturbations of the model. Following White and Boland (1991), we analyzed the resolving power of the obtained model using the SVD of the corresponding matrix of normal equations. To distinguish between the resolved parameter subspace and the null space, we applied a sharp cutoff to the singular value spectrum. No analytic method of finding the appropriate cutoff threshold exists (see, e.g., Firbas, 1987; Koch, 1992). Choosing the right value can be achieved by analyzing the singular-value spectrum and the trade-off curve of model resolution and model variance. The sharp cutoff in the singular-value spec-

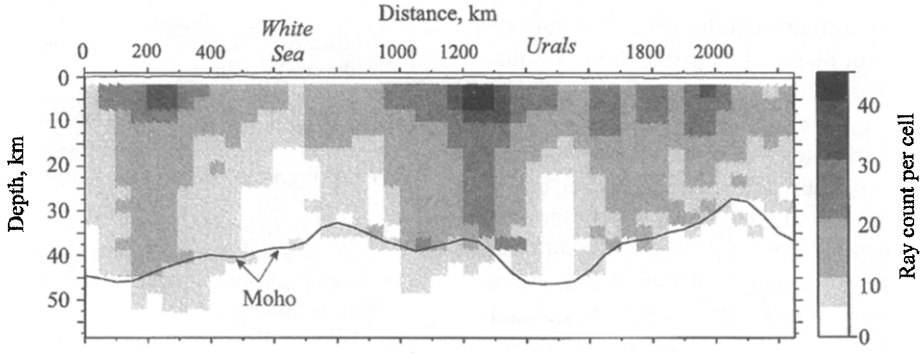

Figure 5. Ray density of final velocity–interface model. The image also represents the sampling used in the inversion. With the exception of the gaps under the White Sea and Urals, the lower crust has an acceptable coverage.

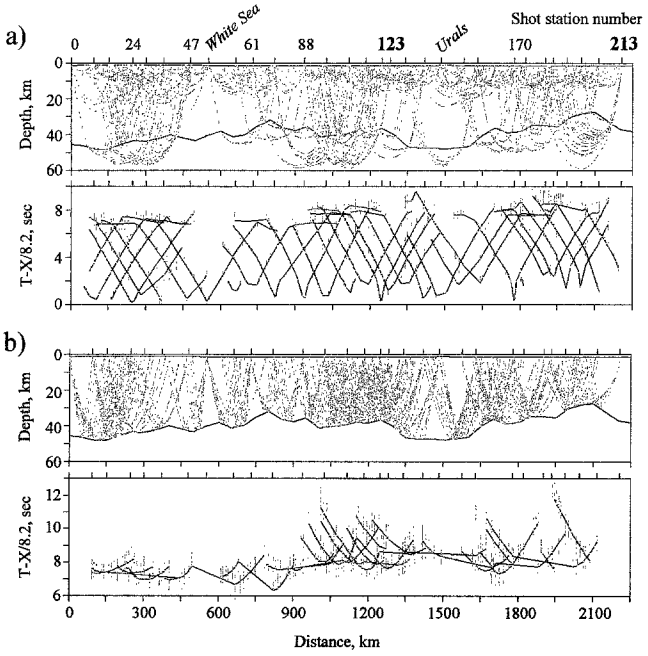

Figure 6. (a) Refracted rays corresponding to all 30 shots used in our analysis traced in the final field velocity model. Corresponding travel-time curves plotted with reduction velocity of 8.2 km/sec are shown under the ray diagram. Solid lines indicate calculated values; error bars represent the uncertainty of travel-time picks. (b) Rays reflected from Moho, traced in the final velocity model, plotted in the same way as in (a).

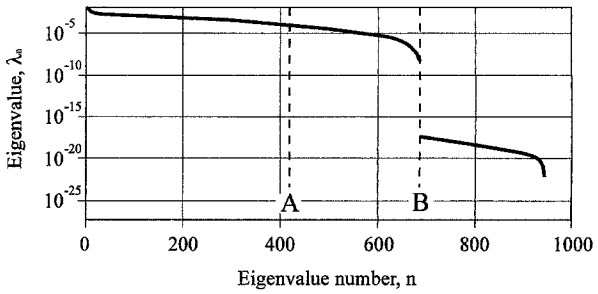

Figure 7. Sorted singular values of the matrix of normal equations. Note two cutoff levels: (A) Value $\lambda \approx 10^{-4}$ determined from the examination of the trade-off between the averaged model resolution and covariance (Fig. 8). This value was used as a damping level in LSQR inversion and in the calculations of the model resolution. (B) Threshold corresponding to the transition from the illuminated to not illuminated part of the velocity model.

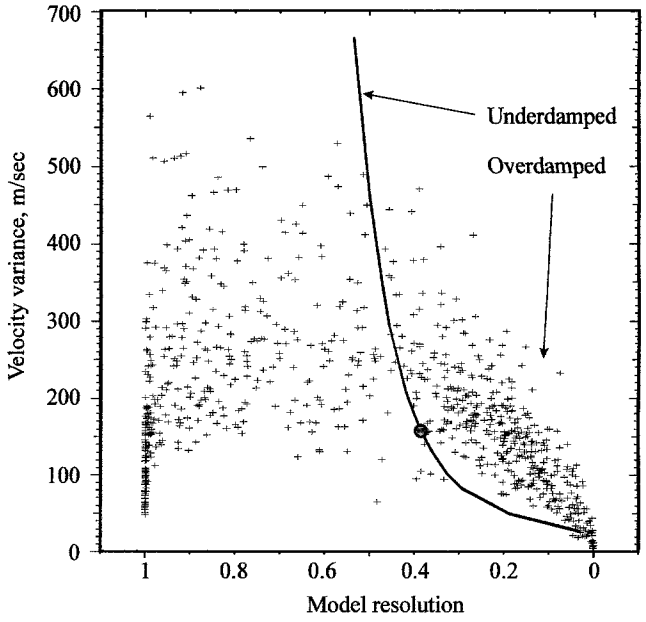

Figure 8. Trade-off between the model resolution and model variance. The solid line represents the variation of the mean values of the diagonal elements of the resolution matrix **R** and the covariance matrix **S** with the change of the minimum singular value ε used in the inversion. The level of damping ε changes from $\varepsilon = 2 \times 10^{-5}$ (upper end of the curve) to $\varepsilon = 10^{-3}$ (lower end). The circle indicates the value $\varepsilon = 10^{-4}$ chosen as the appropriate damping. The scatter plot shows the values of the diagonal elements of the resolution and covariance matrices for all nodes of our final velocity model, calculated using the value $\varepsilon = 10^{-4}$. Note that in the poorer resolved regions, the resolution–variance values concentrate near the lower branch of the trade-off curve, indicating that in these regions, the effective damping is large.

trum at the value $\lambda_{673} \approx 10^{-7}$ (Fig. 7, level B) corresponds to the loss of ray coverage at the bottom and edges of the model. However, the examination of the trade-off curve of model resolution and uncertainty (Fig. 8) shows that the value of the damping parameter $\varepsilon \approx 10^{-4}$ is the appropriate threshold, corresponding to a relatively stable balance between the model resolution and variance. The damping factor used in the last steps of applying the LSQR matrix solver should correlate to the singular-value threshold (White and Boland, 1991). We used the value $\varepsilon \approx 10^{-4}$ as the damping factor in LSQR inversion.

A conventional way to represent the velocity–interface model resolution is to plot diagonal elements of the resolution matrix (Fig. 9). The resulting structure shows the maximum resolution in the upper crust with sections of good to moderate resolution in the lower crust and the uppermost mantle. Most velocity nodes are perfectly constrained down to the depth of approximately 15 km. Only the White Sea area at 550- to 600-km profile distance has low resolution values caused by poor ray coverage. Although the lower crust in the Kola Peninsula, the Timan–Pechora basin, and parts of the west Siberian basin have a dense ray coverage, the angular range is limited to predominantly vertically penetrating rays. Two main crustal structures with poor resolution can be identified: the White Sea area, as already men-

tioned, and the lower crust beneath the Urals. The resolution of the modeled Moho depth correlates with the velocity resolution in the adjacent areas. High values exceeding 0.5 are found in the well-illuminated regions of the Baltic shield and the basin structures surrounding the Uralian belt. Only a small area along the Moho northwest of the Urals reaches resolution values of 1.0. Most other parts of these lower crustal areas have resolution values of 0.5 to 0.9. The Moho is poorly resolved below the White Sea, at the bottom of the crustal depression below the Urals, and at the model edges.

Being a useful tool for estimating the necessary damping, model covariance (Fig. 10) nevertheless cannot be considered as a detailed representation of the obtained velocity uncertainties because of several reasons: (1) the underlying assumption of uncorrelated travel-time uncertainties is not true; (2) as shown below, in poorly resolved areas, the values of the covariance are biased (underestimated) by the damping; and (3) the velocity uncertainties are correlated themselves—therefore, the localized spots of high or low covariance cannot be interpreted independently. An examination of the diagonal elements of the model covariance matrix (Fig. 10) shows that still a surprisingly low-velocity variance of about ± 50 to ± 200 m/sec (velocity uncertainty of 1% to 3%) corresponds to most parts of the lower crust. Most of the well-traversed regions above and below the Moho underneath the White Sea, the Timan–Pechora basin, and the west Siberian basin have uncertainties of ± 200 to ± 300 m/sec. This corresponds to approximately $\pm 3\%$ to $\pm 5\%$ model variance. The depth uncertainty of the modeled Moho boundary is typically less than ± 600 m, which corresponds to depth variations of about $\pm 1.5\%$.

Presented variance estimates are not equally applicable for all regions of the model. To obtain a heuristic criterion of their usability, we inspect the resolution–variance scatter diagram shown in Figure 8. For the resolution values lower then approximately 0.4, the resolution–variance distribution

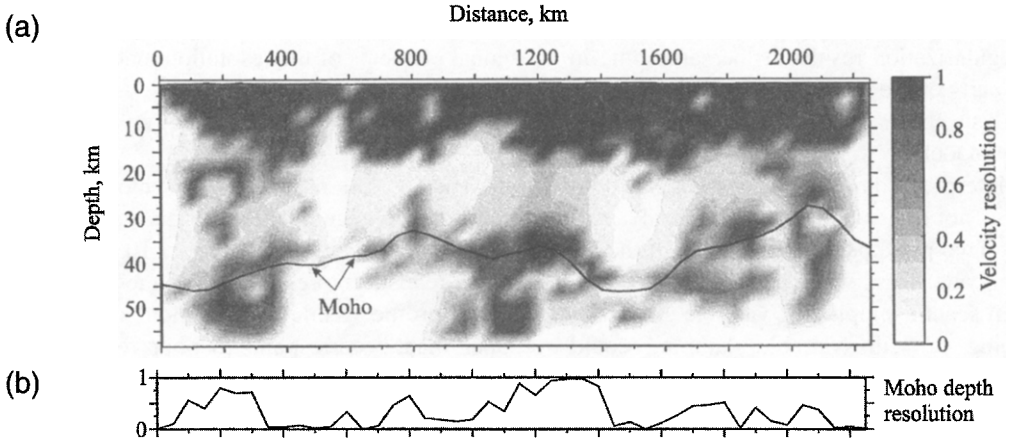

Figure 9. Diagonal elements of the resolution matrix for (a) velocity nodes and (b) Moho depth. Cutoff for singular values is 10^{-4}.

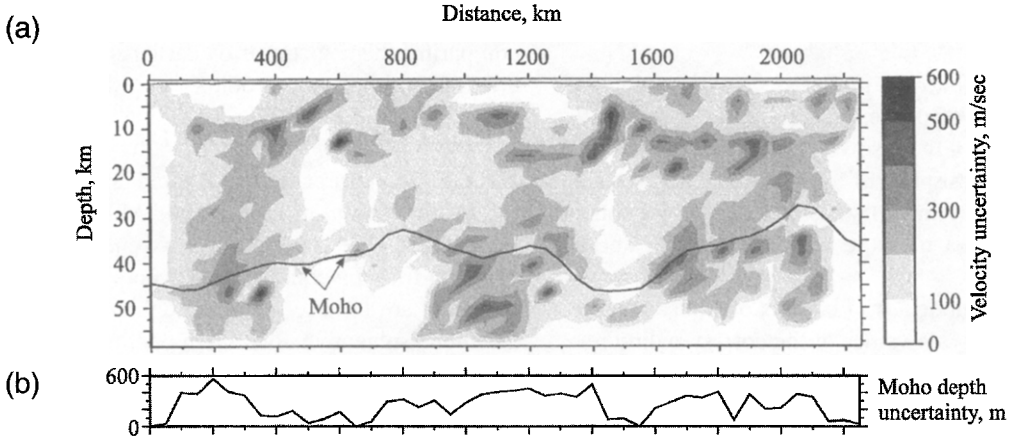

Figure 10. Diagonal elements of the covariance matrix for (a) velocity nodes and (b) Moho depth. Cutoff for singular values is 10^{-4}. Note that low values of the variance in the poorer resolved regions (Fig. 9) are not significant, due to effective overdamping of the inversion in these regions (Fig. 8).

trend follows the "overdamped" branch of the trade-off curve. Although in these regions the velocity and Moho depth variance decreases with decreasing resolution, this decrease in variance is primarily related to the loss of sampling of the model space caused by the damping. Thus, we conclude that the variance estimates are underestimated in the regions where the resolution is below approximately 0.4. Using this criterion, we observe that the velocity variance estimates in Figure 10 represent true velocity uncertainties and are not substantially influenced by the damping only within the top 15 to 20 km of the crust and in the three better-sampled regions near the Moho level (Fig. 9). The same criterion applies to the Moho depth, leaving only two regions with unbiased estimates of the variance—under the Baltic shield and under the Timan belt. Even in these regions, the Moho depth uncertainty appears still very optimistic—about 400 m. This underestimation of the Moho interface depth uncertainty is apparently also mainly caused by the damping. Due to the nonuniform model sampling typical for surface refraction/reflection surveys, and especially pronounced in Quartz dataset, an inversion procedure with a correctly carried out average regularization results at the same time in overdamped lower parts of the model.

The above analysis shows that, although the main features of the velocity model are well constrained and are corroborated by other interpretations of the same data, the conventional approach is not quite adequate for the analysis of the Quartz data set. Two principal improvements of the inversion scheme are made. First, we expect that a more sophisticated inversion scheme employing variable grid spacing without damping or with variable damping could improve the resolution of the model. The discussion of such a scheme is beyond the scope of this article. Second, other useful resolution measures can be derived from the structure of the resolution kernel. One of such measures, showing the spatial extents of the velocity features resolved by the inversion, is described below.

Spatial Resolution Estimation

As we go deeper into the model, decreasing values of the diagonal elements of the resolution matrix do not indicate the spatial extent of the resolved features. It is desirable to have a quantitative estimate of the horizontal and vertical spatial resolution of the model structure. Below we obtain such a description as a measure of the resolution kernel smearing.

For each velocity node i, we find a set of adjacent nodes having the sum of absolute values of the corresponding resolution kernel elements exceeding a certain threshold. The threshold was chosen as 50% of the sum of the absolute values of all elements in the corresponding row of the resolution matrix. This procedure results in a set of adjacent nodes that represents the pattern of spatial smearing of the model resolution at the node point i. The lateral and vertical extents of this distribution are the simplest natural measures of the spatial localization of the velocity features detected by the inversion (Fig. 11).

Well-illuminated model sections like the upper crust and parts of the lower crust (Kola Peninsula, Timan–Pechora basin, and west Siberian basin) are characterized by a low level of spreading that is close to the grid cell spacing. Note that although high resolution matrix diagonals were associated with the lower crust and upper mantle structures below the Baltic shield and the basins northwest and southeast of the Urals, their spatial resolution is only moderate. In addition, the vertical resolution improves in well-covered parts of the uppermost mantle due to a predominantly horizontal ray propagation, and the horizontal resolution decreases due to the same reason. The fact that most large-scale structural elements of horizontal and vertical spreading correlate with each other, especially in the upper crust, indicates that these model regions have a moderate level of ray crisscrossing. Note that the localized spots of poor velocity variance in the upper crust (Fig. 10; e.g., below 1400 to 1500 km of the model distance) correspond to a pronounced loss of the spatial resolution—a fact not so readily observed from the diagonal elements of the resolution matrix (Fig. 9).

Discussion

The resolution analysis presented above allows judgment of the significance of the final velocity–interface model. The velocities in the upper 10 to 20 km of the model give a realistic representation of the upper crust along the Quartz profile. While wide sections of the lower crust and upper mantle correspond to poor resolution values (e.g., White Sea area, Uralian lower crust, and model edges), other areas show a reasonable spatial resolution. These structures include the lower crust and uppermost mantle of the northeastern Baltic shield, the southern Timan–Pechora basin, and sections of the west Siberian basin. For the areas with insufficient resolution, modeled velocities and interface depths are of little significance.

In the following sections, we summarize our results, comparing them to those of earlier studies of the regions crossed by the Quartz profile.

Earlier Modeling of Quartz Data

Our reinterpretation presented above and the earlier GEON interpretation (Egorkin and Mikhaltsev, 1990; Egorkin, 1992) can be considered as two end-member approaches to travel-time inversion. The advantageous features of our approach are (1) use of tomographic inversion rather than the more subjective forward modeling, (2) control of the quality and of the spatial resolution of the obtained model, and (3) the uniform type of model parameterization providing freedom from any assumptions of a block-layer structure of the crust.

Despite these differences in approaches, the model by Egorkin and Mikhaltsev (1990) shows major correlations with the model resulting from our tomographic inversion.

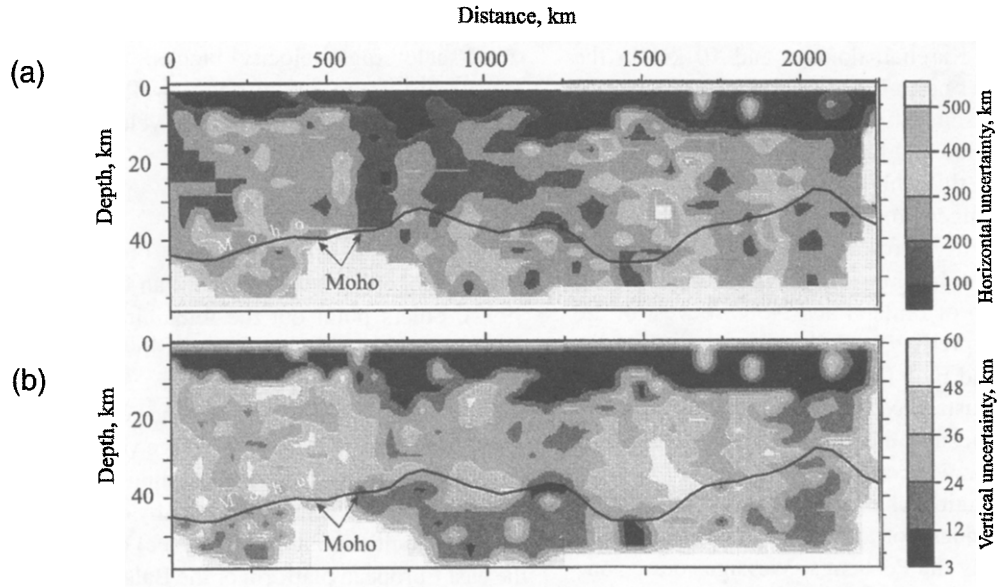

Figure 11. Estimates of spatial resolution in (a) horizontal and (b) vertical directions, obtained by the measurement of the spatial spread of the resolution matrix. See the text for discussion.

Above average crustal velocities, a high-velocity lower crustal block (V_p = 7.0 to 7.4 km/sec), and a deep Moho characterize the Kola Peninsula. Egorkin (1992) also shows a thin (2 to 4 km) low-velocity layer immediately above the Moho at the northern Kola Peninsula, which is not present in our tomographic result. Considering the resolving power of our model, such a thin layer would hardly be recognizable at this crustal depth. Only the central part of the peninsula shows moderately to well-resolved model features, and even at these areas, the vertical spatial resolution is much larger than 3 to 4 km. In agreement with our results, an area of relatively low velocity is present in the earlier model of the upper crust of the southern Timan–Pechora basin with velocities of 5.8 to 6.2 km/sec. The crustal root beneath the Urals is confirmed with a depth of about 48 km and relatively high lower crustal velocities. The velocities below the Moho range from 8.5 to 8.8 km/sec. These very high velocity values exceed those obtained in our tomographic inversion considerably. Also, our spatial resolution analysis shows that sharp lateral velocity contrasts proposed by Egorkin and Mikhaltsev (1990) cannot be resolved from the travel-time data. Thus, although their model lies within the suite of models explaining the travel times, its specific structure depends on the accepted mode of interpretation. On the contrary, we believe that every result of inversion should be accompanied by an analysis of obtained resolution and by a characterization of the suite of possible models.

Crustal Structure of Eastern Fennoscandia

A number of detailed crustal investigations have been carried out on the Baltic shield incorporating numerous geophysical techniques. Korja *et al.* (1993) presented contour maps of the three-dimensional structure of the Moho and the thickness of the high-velocity layer in the lower crust. Values of crustal thickness in the Kola Peninsula range from less than 38 km in the south to about 44 km in the north. This correlates very well with our model results. Further, the thickness of the high-velocity body is estimated to be less than 4 km in the south and far north with a maximum of 14 km in the north-central part of the peninsula. Korja *et al.* show a decreasing thickness toward the northwest, at the far northern end of our model. This feature is not sampled and could not be resolved in our model.

Vertical growth of continental crust results from collision and subduction processes or anorogenic magmatic underplating. Korja *et al.* (1993) assume the formation of the deep crustal high-velocity layer through reworking of the Moho in early Proterozoic, creating a crustal–mantle boundary of age 2.0 to 2.2 Ga. Extension of the Archean crust coincided with the formation of a mafic, lower crustal, high-velocity layer beneath the cratonized crust. Further crustal thickening occurred when a Svecofennian island arc collided with the Archean craton during a period of increased subduction in the Svecofennian orogeny (1.76 to 1.9 Ga). The separate evolution of Archean and Proterozoic crust proposed by Durrheim and Mooney (1991) is not well supported by this model considering (1) the amount of reworking of Archean crust in early Proterozoio; (2) the crustal thickness exceeding 40 km in the central Kola Peninsula (Korja *et al.*, 1993); and (3) the clear presence of a significant lower crustal high-velocity layer along the peninsula. The presence of this layer of a significant thickness is confirmed by most seismic profiles collected in the last 15 to 20 yr covering sections of the eastern Baltic shield (Korhonen *et al.*, 1990; Sharov *et al.*, 1990). All three tectonic domains (Svecofennian, Karelian, and Archean) crossed by the Baltic profile

show this layer reaching a maximum thickness of approximately 25 km in the Karelian domain and 10 km in the Archean domain farther north (Luosto *et al.,* 1990). A similar crustal structure resulted from the interpretations of the 1981 Sveka profile (Grad and Luosto, 1987; Luosto, 1991).

A continuous and thick high-velocity layer not only is present below the younger Proterozoic crust in the south of the profile but also clearly is resolved below the Archean in the north. In 1985, the 440-km-long Polar profile was recorded in the far north of Finland and Norway west of the Kola Peninsula. Interpretive modeling by Luosto *et al.* (1989) and Walther and Flüh (1993) reveal the existence of a significant lower crustal layer with velocities exceeding 7.0 km/sec in the Archean of the northern part of the profile less than 100 km to the west of the Quartz line.

Geotectonic separation of the Kola Peninsula in large-scale tectonic blocks does not appear in our final velocity model. In the same way the Pechenga–Varzuga suture zone and the North–Karelian megashear cannot be followed into deeper parts of the crust, the tectonic units crossed by the profile Quartz (Sørvaranger, Kola, and Belomoria block) do not result in specific velocity discontinuities. Although lateral velocity variations are present in our model, no obvious correlation to the proposed location of these tectonic units can be established.

Seismic profiling along the Kola Peninsula was very limited until about 20 yr ago. In the early crustal model by Sollogub *et al.* (1973), the Moho depth of 36 to 38 km was modeled along the Imandra–Varzuga fold belt in the south. The two-dimensional structure of the Moho boundary given by Glaznev *et al.* (1989) shows its increasing depth from the southeast to the northwest (36 to 41 km), estimated from seismic, gravity, heat flow, and magnetic data. Crustal thickness and lower crustal velocities are poorly constrained. The results by Glaznev *et al.* (1989) do not correspond very well with our velocity model; in particular, no high-velocity layer in the deep crust was obtained in their model. Reaching 46 km in the far north, our model resulted in a generally deeper Moho interface. Luosto *et al.* (1989) also point out this discrepancy between most interpretations of the lower crust from seismic profiles in eastern Fennoscandia and conclusions from Russian data.

While most seismic models of northeastern Fennoscandia show clear evidence for a relatively thin but well-resolved high-velocity layer in the lower crust of the Archean, most interpretations of older Russian data do not indicate this. Although the resolved layer in the ancient parts of the shield is thinner and seems discontinuous, its presence nevertheless appears real. Finally, earlier modeling of the Quartz data and this investigation support the existence of a high-velocity layer as previously outlined. Although no such continuous layer results from the study by Egorkin and Mikhaltsev (1990), distinct sections of high velocities are present in their block-shaped model. High values (>0.6) of the model resolution matrix diagonals from our SVD analysis support the proposed existence of the high-velocity structure. While limited spatial resolution cannot confirm a set of small-scale, high-velocity blocks, the modeled velocity range from 7.0 to 7.4 km/sec is well supported by the resolution analysis and the resulting velocity uncertainties.

Uralian Crustal Root

While most observers agree on the existence of the crustal thickening below the Uralian fold belt (Ryzhiy *et al.,* 1992), others point out the remaining uncertainties in the recognition of a continuous northwest depression in the Moho boundary (Juhlin *et al.,* 1995). According to Belousov and Pavlenkova (1992), the presence of high-velocity bodies in the middle crust result in average velocities in the Uralian crust higher than in the surrounding cratons. This distinct velocity structure is not supported by our modeling. Average crustal velocities (6.5 to 6.6 km/sec) do not exceed those of the east European platform or the Baltic shield. Most seismic profiles covering the fold belt are located in the middle and southern Urals. As a part of the 11 major transects, some of which are described by Tavrin and Khalevin (1990), the Quartz profile crosses the northern section of the orogen. Their models, and also the models by Antonyev *et al.* (1992), result in deep Moho boundary reaching 45 to 50 km in average with the maximum of 65 km underneath the fold belt. High lower crustal velocities are present all along the line and range from 7.4 to 7.8 km/sec in the axial region.

Crustal Models of Sedimentary Basins

According to Belousov and Pavlenkova (1992), sedimentary basins in the territory of the former USSR are generally characterized by a significant thickness of the sedimentary cover (up to 15 to 20 km), crustal thinning in relation to the surrounding platform areas and fold belt systems, and relatively high velocities of the consolidated crust. Zonenshain *et al.* (1990) mention the importance of extensional processes within large aulacogens in the early history of the Timan–Pechora and west Siberian basins causing subsidence of the continental basement structure and subsequent filling with clastic sediments. Deep sedimentary basins are associated with a shallow Moho boundary caused by significant crustal thinning. While our modeled structure of the southern Timan–Pechora basin shows a relatively thin crust (not exceeding 37 km) and a moderately thick sedimentary cover (3 to 4 km), crustal velocities, especially in the upper crust, are comparatively low. No increased average crustal velocities result from our modeling. The modeled shallow Moho (34 to 37 km) east of the Uralian belt corresponds to a sedimentary cover of 2 to 5 km thickness. Velocities in the consolidated crust are similar to the results by Egorkin *et al.* (1987) and do not represent a distinct change in average velocities compared to the Uralian fold belt. Average upper and lower crustal velocities are, however, larger than in the Timan–Pechora basin.

Conclusions

Application of a two-dimensional tomographic inversion to a 2250-km-long segment of the Quartz profile extending from the Kola Peninsula to the west Siberian basin in northwestern Russia resulted in a model for crustal and uppermost mantle *P*-wave velocity structure and the depth of the Moho discontinuity. The final velocity–interface model shows major lateral velocity inhomogeneities in the crust as well as significant variations in Moho depth.

Resolution analysis shows that maximum resolved dimensions of inhomogeneities are close to the grid cell spacing in most sections of the upper crust, in deeper parts of the model structure, they reach values of 3 to 6 grid cells (150 to 300 km) horizontally and 2 to 12 grid cells (6 to 36 km) vertically. The regions with low spatial resolution are sampled by subparallel rays. We demonstrate that a conventional inversion scheme with a single damping parameter is always overdamping the poorer sampled regions of the model, also leading to the loss of the spatial resolution. As expected, denser ray coverage and a wider angular range in the upper part of the model results in a much better resolution in the upper crustal structure than in the lower crust and uppermost mantle. Spatial resolution generally degenerates with increasing model depth. Uncertainties of the modeled velocities range from 200 to 300 m/sec, which is equivalent to 3% to 5% model error.

Resolution analysis confirms the modeled high-velocity structure in the lower crust and a deep Moho beneath the Kola Peninsula. *P*-wave velocities exceed 7.0 km/sec at 27 to 31 km depth and reach maximum values of 7.4 km/sec in the lowermost crust. Depths of the Moho range from 40 to 47 km. This crustal feature is confirmed by a number of other geophysical studies in the region, and its origin can be explained as the result of underplating during continental collision in the early Proterozoic. The basin structures show a moderate to thick layer of sedimentary rock (2 to 5 km) and a corresponding crustal thinning to 35 km in average. Although we did not observe increased velocities in the upper and lower crust under the Timan–Pechora and the west Siberian basins, both basin structures correlate with established models of sedimentary basin formation, i.e., significant volumes of sedimentary rocks associated with crustal thinning in these areas. Crustal roots are detected under the Timan and the Ural fold belts reaching maximum depths in the axial regions of 38 and 46 km, respectively. While the quality of ray coverage and the resulting resolution beneath the fold belt structures is not very high, the presence of crustal thickening in these regions is well established.

Compared to the analysis by Egorkin and Mikhaltsev (1990), our modeling shows major similarities in high velocities in the northeastern Baltic shield, the deep Moho underneath the fold belts, and crustal thinning under the deep sedimentary basins. Our spatial resolution analysis, however, shows that due to the nature, volume, and density of the available travel-time data, it is hardly possible to resolve the proposed existence of a fine-scaled, block-layered structure with sharp lateral velocity contrasts and deep penetrating fault zones. From the available travel-time data, such a mosaic-like pattern seems beyond the limit of what we can expect to resolve.

On the other hand, the results of this study show that the potential of tomographic inversion of the Quartz crustal data set is not exhausted. A more versatile parameterization and regularization scheme would allow a better resolution of the upper crust without loss of the velocity control in the lower regions.

Acknowledgments

The acquisition of the Quartz data set has been a tremendous effort on behalf of Soviet geophysicists, and especially of the staff of the Center GEON (Special Geophysical Expedition at the time of data acquisition). We are grateful to Director L. Solodilov, E. Kazachenko, O. Ganzha, and other specialists of GEON who digitized the data and provided other necessary information, including earlier travel-time picks. We also thank N. Pavlenkova (Institute of Physics of the Earth, Moscow), who shared with us her experience of the interpretation of Quartz and other DSS data. We thank D. J. White of the Canadian Geological Survey for providing his codes to perform raytracing and iterative matrix solving, and W. D. Mooney (USGS) for several discussions of the results. The remarks by two anonymous reviewers were very helpful for the improvement of the manuscript.

Our work on this project was sponsored by the Air Force Office for Scientific Research under Grant F49620-94-1-0134. One of us (I.M.) was also supported in part by NSF Grant EHR-910-8774-02.

References

Avtoneyev, S. V., Y. M. Anan'yeva, K. G. Bashta, O. V. Bellavin, Y. P. Bulashevich, V. S. Druzhinin, A. G. D'yakonova, K. K. Zoloyev, V. V. Kolmogorova, V. A. Koroteyev, F. I. Nikonova, B. A. Popov, V. N. Puchkov, M. S. Rapoport, V. M. Rybalko, B. P. Ryzhiy, B. G. Semenov, I. F. Tavrin, A. M. N. Tiunova, N. V. Fedorova, Y. V. Kachray, A. V. Chursin, V. A. Shapiro, and V. A. Shchapov (1992). Deep structure of the Urals from geophysical data, in *Structure of the Crust and Upper Mantle of the (Former) USSR,* V. V. Belousov, N. I. Pavlenkova, and G. N. Kvyatkovskaya (Editors), Part I, Chap. 5, *Int. Geol. Rev.* **34,** 263–279.

Belousov, V. V. and N. I. Pavlenkova (1992). General features of crustal structure, in *Structure of the Crust and Upper Mantle of the (Former) USSR,* V. V. Belousov, N. I. Pavlenkova, and G. N. Kvyatkovskaya (Editors), Part II, Chap. 6, *Int. Geol. Rev.* **34,** 416–431.

Benz, H. M., J. D. Unger, W. S. Leith, W. D. Mooney, L. Solodilov, A. V. Egorkin, and V. Z. Ryaboy (1992). Deep seismic sounding in northern Eurasia, *EOS* **73,** 297–304.

Berthelsen, A. and M. Marker (1986). Tectonics of the Kola collision suture and adjucent Archean and early Proterozoic terrains in the northeast region of the Baltic shield, *Tectonophysics* **126,** 31–55.

Braile, L. W., B. Wang, C. R. Daudt, G. R. Keller, and J. P. Patel (1994). Modeling the 2-D seismic structure across the Kenya rift, *Tectonophysics* **236,** 251–269.

Durrheim, R. J. and W. D. Mooney (1991). Archean and Proterozoic crustal evolution: evidence from crustal seismology, *Geology* **19,** 606–609.

Egorkin, A. V. (1992). Crustal structure along seismic geotraverses, in *Structure of the Crust and Upper Mantle of the (Former) USSR,* V. V. Belousov, N. I. Pavlenkova, and G. N. Kvyatkovskaya (Editors), Part II, Chap. 1, *Int. Geol. Rev.* **34,** 345–362.

Egorkin, A. V. and N. I. Pavlenkova (1981). Studies of mantle structure of

USSR territory on long-range seismic profiles, *Phys. Earth Planet. Interior* **25,** 12–26.

Egorkin, A. V., S. K. Zuganov, N. I. Pavlenkova, and N. M. Chernyshev (1987). Results of lithospheric studies from long-range profiles in Siberia, *Tectonophysics* **140,** 29–47.

Egorkin, A. V. and A. V. Mikhaltsev (1990). The results of seismic investigations along geotraverses, in *Super-Deep Continental Drilling and Deep Geophysical Sounding,* K. Fuchs, Y. A. Kozlovsky, A. I. Krivtsov, and M. D. Zoback (Editors), Super-Deep Continental Drilling and Deep Geophysical Sounding, Springer, Berlin, 111–119.

Egorkin, A. V., I. P. Kosminskaya, and N. I. Pavlenkova (1991). Multisided seismic investigations of continental lithosphere, *Izv. Earth Phys.* **27,** 793–803.

Firbas, P. (1987). Tomography from seismic profiles, in *Seismic Tomography,* G. Nolet (Editor), Reidel, Dortrecht, 189–202.

Glaznev, V. N., A. B. Raevsky, and N. V. Sharov (1989). A model of the deep structure of the northeastern part of the Baltic shield based on joint interpretation of seismic, gravity, magnetic and heat flow data, *Tectonophysics* **162,** 151–163.

Grad, M. and U. Luosto (1987). Seismic models of the crust of the Baltic shield along the SVEKA profile in Finland, *Ann. Geophys.* **5B,** 639–650.

Juhlin, C., S. Kashubin, J. H. Knapp, V. Makovsky, and T. Ryberg (1995). Project conducts seismic reflection profiling in the Ural mountains, *EOS* **76,** 193–199.

Koch, M. (1992). Optimal Regularization of the Linear Seismic Inverse Problem, in *Geophysical Inversion,* J. B. Bednar (Editor), SIAM, Philadelphia, Pennsylvania, 183–245.

Korhonen, H., I. P. Kosminskaya, I. Azbel, N. Sharov, V. Zagorodny, and U. Luosto (1990). Comparison of crustal structure along DSS profiles in SE Fennoscandia, *Geophys. J. Int.* **103,** 157–162.

Korja, A., T. Korja, U. Luosto, and P. Heikkinen (1993). Seismic and geoelectric evidence for Collisional and extensional events in the Fennoscandian shield—implications for Precambrian crustal evolution, *Tectonophysics* **219,** 129–152.

Kozlovsky, Y. A. (1990). The USSR integrated program of continental crust investigations and studies of the Earth's deep structure under the Globus project, in *Super-Deep Continental Drilling and Deep Geophysical Sounding,* K. Fuchs, Y. A. Kozlovsky, A. I. Krivtsov, and M. D. Zoback (Editors), Springer, Berlin, 90–103.

Lutter, W. J. and R. L. Nowack (1990). Inversion for crustal structure using reflections from the PASSCAL Quachita experiment, *J. Geophys. Res.* **95,** 4633–4646.

Luosto, U. (1991). Crustal structures of eastern Fennoscandia, *Tectonophysics* **189,** 19–27.

Luosto, U., E. R. Flüh, C. E. Lund, and Working Group (1989). The crustal structure along the POLAR profile from seismic investigations, *Tectonophysics* **162,** 51–85.

Luosto, U., T. Tiira, H. Korhonen, I. Azbel, V. Burmin, A. Buyanov, I. Kosminskaya, V. Ionkis, and N. Sharov (1990). Crust and upper mantle structure along the DSS Baltic profile in SE Finland, *Geophy. J. Int.* **101,** 89–110.

Mechie, J., A. V. Egorkin, K. Fuchs, T. Ryberg, L. Solodilov, and F. Wenzel (1993). P-wave mantle velocity structure beneath northern Eurasia from long-range recordings along the profile Quartz, *Phys. Earth Planet. Interior* **79,** 269–286.

Nalivkina, E. B., M. S. Rusanov, and S. N. Suslova (1987). Geology of the north-eastern Baltic shield, in *The Superdeep Well of the Kola Peninsula,* Y. A. Kozlovsky (Editor), Springer, Berlin, 17–39.

Nolet, G. (1985). Solving or resolving inadequate and noisy tomographic systems, *J. Comp. Phys.* **61,** 463–482.

Nolet, G. (1993). Solving large linearized tomographic problems, in *Seismic Tomography, Theory and Practice,* H. M. Iyer and K. Hirahara (Editors), Chapman and Hall, London, 227–247.

Pavlenkova, N. I. (1992). Some general features of the structure of the lithosphere, in *Structure of the Crust and Upper Mantle of the (Former) USSR,* V. V. Belousov, N. I. Pavlenkova, and G. N. Kvyatkovskaya (Editors), Part II, Chap. 3, *Int. Geol. Rev.* **34,** 370–382.

Paige, C. C. and M. A. Saunders (1982). LSQR: an algorithm for sparse linear equations and sparse least squares, *ACM Trans. Math. Software* **8,** 43–71.

Ryberg, T., F. Wenzel, J. Mechie, A. Egorkin, K. Fuchs, and L. Solodilov (1996). Two-dimensional velocity structure beneath northern Eurasia derived from the super long-range seismic profile Quartz, *Bull. Seism. Soc. Am.* **86,** 857–867.

Ryzhiy, B. P., V. S. Druzhinin, F. F. Yunusov, and I. V. Ananyin (1992). Deep structure of the Urals region and its seismicity, *Phys. Earth Planet. Interior* **75,** 185–191.

Scales, J. A. (1987). Tomographic inversion via the conjugate gradient method, *Geophysics* **52,** 179–185.

Sharov, N., I. P. Kosminskaya, I. Azbel, V. Zagorodny, H. Korhonen, and U. Luosto (1990). Compiling DSS profiles in the southeast of the Baltic shield, *Geotectonics* **24,** 35–42.

van der Sluis, A. and H. A. van der Vorst (1987). Numerical solution of large, sparse linear algebraic systems arising from tomographic problems, in *Seismic Tomography,* G. Nolet (Editor), Reidel, Dortrecht, 49–83.

Sollogub, V. B., I. V. Litvinenko, A. V. Chekunov, S. A. Ankudinov, A. A. Ivanov, L. T. Kalyuzhnaya, L. K. Kokorina, and A. A. Triplosky (1973). New D.S.S. data on the crustal structure of the Baltic and Ukrainian shields, *Tectonophysics* **20,** 67–84.

Spakman, W. and G. Nolet (1988). Imaging algorithms, accuracy and resolution in delay time tomography, in *Mathematical Geophysics,* N. J. Vlaar, G. Nolet, M. J. R. Wortel, and S. A. P. L. Cloetingh (Editors), Reidel, Dortrecht, 155–187.

Tavrin, I. F. and N. I. Khalevin (1990). Geophysical models for the Ural crust, *Geotectonics* **24,** 223–229.

Tichelaar, B. W. and L. J. Ruff (1989). How good are our best models?—Jackknifing, bootstrapping, and earthquake data, *EOS* **70,** 599–606.

Volkov, V. M., A. N. Eremeev, A. S. Kireev, L. I. Krasny, G. V. Kulikov, N. V. Mezhelovsky, and Y. M. Pushcharovsky (Editors) (1984). *Geology of the USSR, 27th Int. Geol. Congress,* Moscow.

Walther, C. and E. R. Flüh (1993). The POLAR profile revised: combined P- and S-wave interpretation, *Precambrian Res.* **64,** 153–168.

White, D. J. (1989). Two-dimensional seismic refraction tomography, *Geophys. J.* **97,** 223–245.

White, D. J. and A. V. Boland (1991). A comparison of forward modeling and inversion of seismic first arrivals over the Kapuskasing uplift, *Bull. Seism. Soc. Am.* **82,** 304–322.

White, D. J. and R. M. Clowes (1990). Shallow crustal structure beneath the Juan de Fuca ridge from 2-D seismic refraction tomography, *Geophys. J. Int.* **100,** 349–367.

Zhang, J. and G. A. McMechan (1995). Estimation of resolution and covariance for large matrix inversions, *Geophys. J. Int.* **121,** 409–426.

Zhou, H., J. A. McDonald, C. A. Link, and J. Jech (1993). Constraining the magnitude of velocity perturbations in travel time tomography, *J. Seismic Exploration* **2,** 365–380.

Zonenshain, L. P., M. I. Kuzmin, and L. M. Natapov (1990). *Geology of the USSR: A Plate Tectonic Synthesis, AGU Geodynamics Series, Volume 21,* American Geophysical Union, Washington, D.C.

Department of Geology and Geophysics
University of Wyoming
P.O. Box 3006
Laramie, Wyoming 82071-3006

Manuscript received 20 February 1996.